

Bond Model of Dilated Polyhedral DEM and its Applications in Sea Ice Simulation

First author¹, second author², third author² (First name + Middle initial + Last name)

State Key Laboratory of Structure Analysis of Industrial Equipment, Dalian University of Technology, Dalian 116023, China

ABSTRACT

The simulation of breaking process of continuum is an important issue for discrete element method. An explicit bonding method is developed based on Rigid Body Spring Method (RBSM) to simulate fracture with Dilated-polyhedron DEM (DP-DEM) in this paper. Minkowski sum of basic polyhedron and sphere is used to generate the dilated polyhedral element. Bond points are fixed on the common face between elements. Each bond point represents average area of the common face. The strain on every bond point is calculated by the division of distance between bond points and characteristic length. Then the stress can be determined according the stiffness in RBSM. The bond force at bond point is evaluated by stress and average area of every bond point. So the resultant force and moment of each element could be obtained by summation of force at each bond point and its moment to mass center. The complex matrix calculation and the integral for stiffness in RBSM could be avoided to save computational resources. The fracture on the interface is decided by Mohr-Coulomb criterion. After the fracture, DEM would take charge of the broken element in contact computation. This method is built to simulate the fracture of sea ice interacting with structure. The ice loads on structure and broken ice shape is analyzed to measure the applicability of this method in sea ice simulations.

KEY WORDS: Bonding model, Dilated polyhedral DEM, Sea ice, Breaking process, Ice loads

1. INTRODUCTION

Since the discrete element method (DEM) has been acknowledged to be a valid method to study granular matter, the studies of simulating fragmentation of brittle material with DEM have obtained a lot of attentions for its simple mathematical model and parallel algorithm (Potyondy and Cundall, 2004). However, sphere-based DEM has drawbacks because of the intervals inside the assembly of spheres. Therefore, the polygonal/polyhedral element is still widely used in DEM (Hopkins, 2014).

Minkowski sum is introduced to generate dilated polyhedron with tunable grain roundness (Mollon and Zhao, 2012). This method avoids the singularity of corner contact pattern and the choice of contact points (Pournin and Liebling, 2005). Due to the dilated part in geometry, the contact detection could overcome the unphysical behavior of multiple simultaneous contacts. Based on dilated polyhedral element, Galindo-Torres (2012) developed a bond model to simulate fracture of material by an appropriate failure criterion. However, the stress and strain on the cohesive interface are evaluated inappropriately in the bond model (Gerolymatou et al., 2015). Besides, the parameters used in this model can only be determined by a series of numerical tests.

Finite Element Method (FEM) is employed with DEM to analyze breaking process named as coupled FEM-DEM model (Munjiza et al., 2014) due to the calculative precision of stress and strain. The Rigid Finite Element Method (RFEM), or called as Rigid Body-Spring Method (RBSM) (Kawai, 1978; Zhang, 1999) builds cohesion on the interface between adjacent elements. This method uses displacement of every element mass center as the degree of freedom, while the stress precision can be maintained at the same level with displacement precision. The coupled RBSM and DEM method is successful in simulating concrete failure process (Zhang et al., 2001; Nagai et al., 2005). Thus RBSM is an effective numerical way to study failure process.

DEM and FEM, and their coupling method are valid ways to study ice failure and ice loads. The dilated disk element is used to simulate floe ice jam in a river, which is similar with dilated polyhedral element (Hopkins, 2004). The coupled FEM-DEM method is adopted in ridge keel punch through tests by modelling freeze bonds between ice blocks (Polojärvi and Tuhkuri, 2013). The crack propagation by wing crack model in ice is studied by FEM (Kolari, 2015). Through numerical tests of compression and bending, the parameters of parallel-bond model of spherical element in DEM are studied to analyze the ice loads on structure (Ji et al., 2016). These numerical approaches become more and more important in engineering.

RBSM is modified as an explicit algorithm in this paper. Then it is adopted in dilated polyhedral DEM (DP-DEM) to simulate interaction between ice and conical structure. The ice loads on structure is analyzed and compared with field data of Bohai Sea.

2. NUMERICAL METHODOLOGY

Minkowski sum theory is used to generate the dilated polyhedral element (Ji et al., 2016). DEM with the dilated polyhedral element is established. Hereby RBSM is modified by abandoning matrix calculation, which fits to insert to the data structure in DEM.

2.1. Dilated Polyhedral DEM

The nature of Minkowski sum theory means sweeping one geometric shape around the profile of the other. The dilated polyhedron is the result of Minkowski sum by a basic polyhedron and a sphere, i.e., the sphere sweeps on the profile of the basic polyhedron, shown in Figure 1.

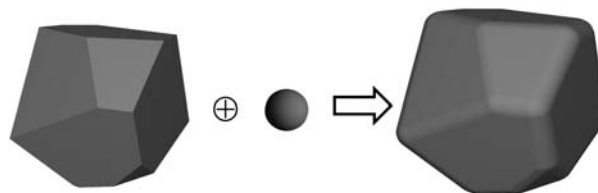


Figure 1. The dilated polyhedron generated by a basic polyhedron and a sphere.

Due to the dilated part in geometry, the profile of dilated polyhedron is smooth curve, including sphere, cylinder and flat face. The contact force model could be built by Hertz Model (Liu et al., 2016).

The normal force between them can be modelled by considering the elastic force caused by normal elastic deformation and the normal viscous force caused by relative velocity as viscoelasticity model:

$$F_n = k_n \delta_n^\kappa + C_n \delta_n^{\kappa-1} \dot{\delta}_n \quad (1)$$

where k_n is normal contact stiffness which depends on specific contact pattern; κ is usually 1.5 in Hertz model; δ_n and $\dot{\delta}_n$ are normal deformation and normal relative velocity; C_n is normal damping coefficient.

Likewise, ignored tangential viscous force, tangential force is defined by tangential elastic force, and related with friction force:

$$F_s^* = k_s \delta_s^{\kappa-1} \delta_s \quad (2)$$

$$F_s = \min(F_s^*, \text{sign}(F_s^*) \mu F_n) \quad (3)$$

where k_s is tangential stiffness, and $k_s = r_{sn} k_n$. Here r_{sn} is defined as $1/2(1 + \nu)$ according to the relationship between elastic modulus and shear modulus of isotropic material, ν is the Poisson ratio. δ_s is the tangential elastic deformation; μ is friction coefficient.

2.2. Modified RBSM

The integral equilibrium equation of RBSM can be obtained by Galerkin theory, written as

$$\int_S \delta \mathbf{u}^T (\boldsymbol{\sigma} \mathbf{n}) dS + \int_V \rho \delta \mathbf{u}^T (\mathbf{f} - \mathbf{a}) dV = 0 \quad (4)$$

where $\boldsymbol{\sigma}$ is the Green stress tensor, \mathbf{n} is the outer normal vector of the interface between two adjacent elements, S is the area of interface, ρ is the mass density, \mathbf{f} is the mass force, \mathbf{a} is the acceleration, V means the continuum volume, $\mathbf{u} = \{u \ v \ w\}^T$ is the displacement of the mass center.

As shown in Figure 2, the bonds (springs) are established on the point of the common face between the two adjacent elements. The normal and shear force are considered between the two bonded points. In this paper, the bonded points are chosen as the corner points of the common face. The normal strain is evaluated on every bonded point by the following formula

$$\varepsilon_n = \frac{\mathbf{d} \cdot \mathbf{n}}{C} \quad (5)$$

where \mathbf{n} is the normal vector, which is defined as the normal of the angle bisecting plane between the bond faces of the two adjacent elements; C is a scalar named as characteristic length, which is the summation of the distances from element centers to the interface of the two elements, as

$$C = h_m + h_n \quad (6)$$

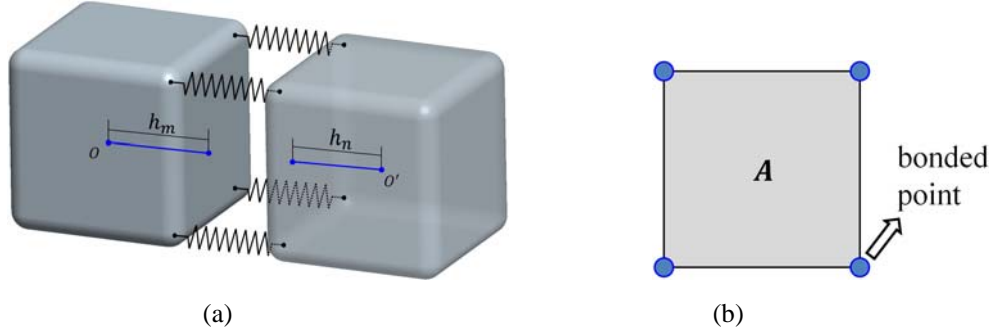


Figure 2. The common face of the adjacent elements: (a) Two adjacent elements; (b) The common face of the two adjacent elements, A is the area of the face.

The shear strain is obtained by

$$\varepsilon_t = \frac{|\mathbf{d} - \mathbf{d} \cdot \mathbf{n}|}{C} \quad (7)$$

The two directions of shear force are considered to compose in only one direction $\mathbf{t} = \text{unit}(\mathbf{d} - \mathbf{d} \cdot \mathbf{n})$, because the shear force would finally be transformed on the mass center. Based on the elastic matrix in RBSM, the stress is calculated by

$$\boldsymbol{\sigma} = \frac{E(1-\mu)}{(1+\mu)(1-2\mu)} \begin{bmatrix} 1 & 0 \\ 0 & \frac{1-2\mu}{2(1-\mu)} \end{bmatrix} \boldsymbol{\varepsilon} \quad (8)$$

where $\boldsymbol{\sigma} = \{\sigma \ \tau\}^T$, $\boldsymbol{\varepsilon} = \{\varepsilon_n \ \varepsilon_t\}^T$. The bond force between two bonded points is

$$\mathbf{F} = \boldsymbol{\sigma} \cdot \frac{A}{n} \quad (9)$$

All bond force between bonded points on the interface would be determined by Eq. (9) and transformed on the mass center. With contact force together, the motion of every element is obtained by explicit integral algorithm.

2.3. Fracture Criterion

Mohr-Coulomb criterion is adopted to detect the failure which is divided in the normal and shear direction separately, see Figure 3. In normal direction, the tensile strength is a given threshold σ_b^n , and the failure in tension is determined by

$$\sigma < \sigma_b^n \quad (10)$$

The shear strength is controlled by the following equation

$$\tau_b = C + \sigma_n \tan \theta \quad (11)$$

where C is cohesion; θ is internal friction angle, $\mu_b = \tan \theta$ is internal friction coefficient; σ_n is the normal stress. Note that tension is negative and compression is positive. With Eq. (11), the compressive stress is related with shear strength. The failure in shear direction is determined by

$$\tau < \tau_b \quad (12)$$

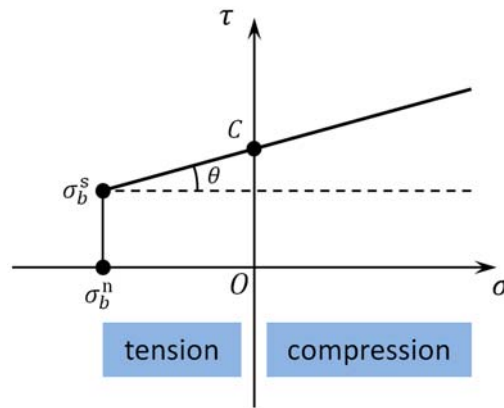


Figure 3. Failure criterion. The normal strength is a given threshold, while the shear strength is related to the compression stress determined as Eq. (11).

Mohr-Coulomb criterion is not quite appropriate for the compressive failure. Other strength criteria, related to stress intensity factor, fracture toughness, etc., could be adopted here to improve the computational accuracy (Gui et al., 2015; Guo et al., 2015).

2.4. Contact Detection

Contact detection is the most cumbersome part which affects the computational efficiency seriously in polyhedral DEM. The detecting time interval is taken into the simulation which means a potential contact list is built and updated at every detecting time interval. The detecting time interval is usually 10~20 times as much as simulating time interval. Besides, because the contact detection is not implemented every time step, the detecting terms need to be softened a little to ensure the accuracy during detecting time interval.

The contact detection is divided into three steps: uniform grid method, filter contact pairs, and detecting contact pattern and contact point. Uniform grid method is widely used in collision detection in game programming, and it is quite efficient in spherical DEM. Filtering the possible contact pair generated in the upper step is the most important step here. Actually this algorithm is developed from the Separation Axis Algorithm (SAA) (Torquato et al., 2009). The main object of the filtering process is to find a face of a polyhedron which all the vertices of the adjacent polyhedron are outside of. Different from traversing all vertices and faces of polyhedra in SAA, this algorithm would break out if the object has already been achieved, which aimed at convex polyhedron technically.

Although a remarkable improvement is provided in the detection part, we still pursue a higher efficient way for contact detection and even the whole simulation process. Thus, the OpenMP, an effective parallel computing technology, is adopted here for element-level parallelization which improve the computational efficiency on the basis of the modified detection method. This parallel level is coarse-grained, and fine-grained parallelization could be built at contact-type-level actually. The fine-grained parallelization would provide a more efficient way, but it requires a more complex data structure to avoid the access conflict in threads (Nishiura et al., 2011), which would also occupy more memory.

3. DP-DEM SIMULATION OF ICE-STRUCTURE INTERACTION

The ice load on conical structure interacting with level ice is simulated by DP-DEM with bond model. The structure is modelled according to the cone pile in Bohai Sea for the comparison between simulation and field data. Figure 4 is a snapshot of the ice breaking

process.

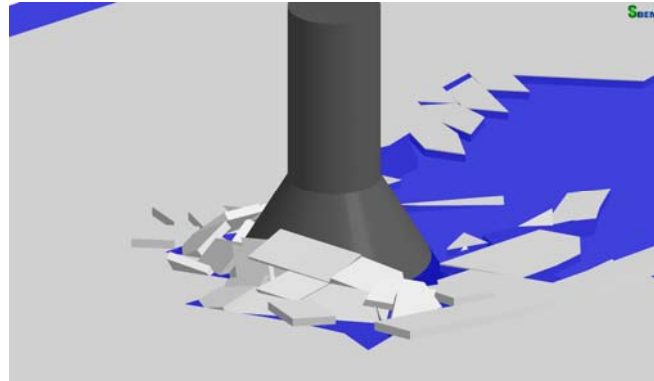


Figure 4. A snapshot of level ice simulation. Obvious bending failure is observed during the ice breaking process in this picture.

Figure 5 is the ice load in x direction when $\sigma_b^n = 1.0$ MPa and $\sigma_b^s = 0.5$ MPa. Comparing the simulation result and the field data in Bohai Sea, the data is shown in Table 2. The ice load exhibits the feature of bending failure, which conforms to Figure 4. The comparison with field data of Bohai Sea is shown in Table 2.

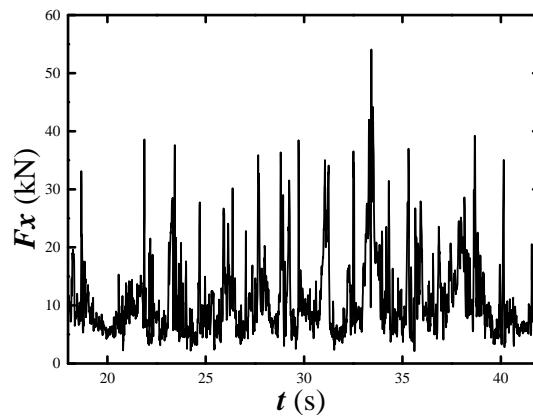


Figure 5. Ice load in x direction: $\sigma_b^n = 1.0$ MPa and $\sigma_b^s = 0.5$ MPa.

The comparison with field data of Bohai Sea is shown in Table 1. The average mean forces are close, while the standard deviation have bigger difference. Obviously bond strengths and their ratio have important effects on the ice load. The approach to choose appropriate strengths requires more specific study on this numerical method. Usually the strengths used in simulation are based on bending and compressive experiments of ice. However, the strengths used in this method have deviation with practical strengths due to the numerical approximation of stress determination. The validation of bond strengths is necessary to evaluate the error of this method.

Table 1. Comparison between DEM results and field data

Definitions	Simulation (kN)	Field data in Bohai (kN)
Average mean force	21.78	29.3
Standard deviation	9.63	21.3

On the other hand, the ice load on conical structure is affected by ice thickness and cone diameter. The ratio between ice thickness (h) and cone diameter (D) is studied by comparing with field data of Bohai Sea, see Figure 6. The numerical results is bigger but close to field results. The ice load in this figure exhibits in linear. However, it cannot be summarized that the ice load is linear with h/D . The ratio changes in the simulation are all due to the change of ice thickness, while the cone diameter keeps the same. In fact, the cone diameter also changes little in the field data. So the cone diameter is not considered severely. But the comparison shows DP-DEM is an effective way to study the ice load on structure.

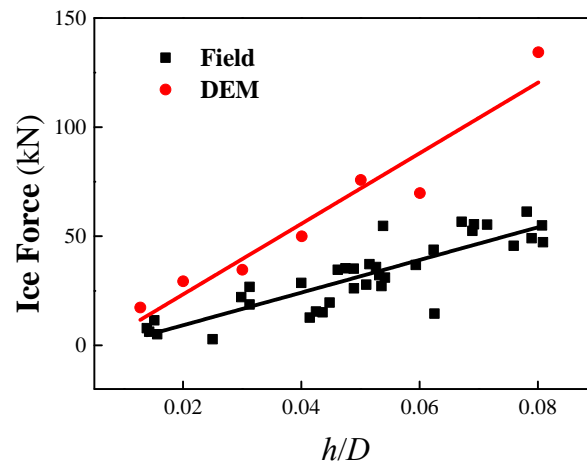


Figure 6. The ice load affected by the ratio between ice thickness and cone diameter. The ice loads in this figure are all maximum value. The field data of Bohai Sea is from Yue et al. (2005) and Qu et al. (2006).

CONCLUSIONS

A bond model modified according to RBSM is introduced with DP-DEM. This method is based on building the cohesion of point pairs on the common face. The elastic matrix in RBSM is employed to determine the bond force between bonded points. Meanwhile, Mohr-Coulomb criterion is adopted to detect the failure process. The stress is detected separately in normal and shear with different strength thresholds. The contact detection of dilated polyhedron is introduced to improve the computational efficiency. This method is used to simulate the interaction between level ice and conical structure. The result is compared with field data of Bohai Sea. Generally, the parameters, especially bond strengths, need more sensibility analysis on ice failure modes.

REFERENCES

- Galindo-Torres S.A., Pedroso D.M., Williams D.J., Li L., 2012. Breaking processes in three-dimensional bonded granular materials with general shapes. *Computer Physics Communications*, 183(2), pp.266-277.
- Gerolymatou E., Galindo-Torres S.A., Triantafyllidis T., 2015. Numerical investigation of the effect of preexisting discontinuities on hydraulic stimulation. *Computers & Geotechnics*, 69, pp.320-328.
- Gui Y.L., Bui H.H., Kodikara J., Zhang Q.B., Zhao J., Rabczuk T., 2015. Modelling the dynamic failure of brittle rocks using a hybrid continuum-discrete element method with a mixed-mode cohesive fracture model. *International Journal of Impact Engineering*, 87, pp.146-155.

- Guo L., Latham J.P, Xiang J., 2015. Numerical simulation of breakages of concrete armour units using a three-dimensional fracture model in the context of the combined finite-discrete element method. *Computers & Structures* 146(7386), 117-142.
- Hopkins M.A., 2004. Discrete element modeling with dilated particles. *Engineering Computations*, 21, pp.422-430.
- Hopkins M.A., 2014. Polyhedra faster than spheres? *Engineering Computations*, 31(3), pp.567-583.
- Ji S., Di S., Long X., 2016. DEM Simulation of Uniaxial Compressive and Flexural Strength of Sea Ice: Parametric Study. *Journal of Engineering Mechanics*, C4016010.
- Ji S., Sun S., Yan Y., 2016. Discrete element modeling of dynamic behaviors of railway ballast under cyclic loading with dilated polyhedra. *International Journal for Numerical & Analytical Methods in Geomechanics*.
- Kawai T., 1978. New discrete models and their application to seismic response analysis of structures. *Nuclear Engineering & Design*, 48(1), pp.207-229.
- Kolari K., 2015. Simulation of the temperature and grain size dependent uniaxial compressive strength using 3D wing crack model. In: Thronheim, Norway, *Proceedings of the 23rd International Conference on Port and Ocean Engineering under Arctic Conditions*.
- Liu L., Sun S., Ji S., 2016. Interaction Between Floater and Sea Ice Simulated with Dilated Polyhedral DEM. In: Dalian, China, *Proceedings of the 7th International Conference on Discrete Element Methods*, Volume 188 of the series Springer Proceedings in Physics, pp.1065-1074.
- Mollon G., Zhao J., 2012. Fourier–Voronoi-based generation of realistic samples for discrete modelling of granular materials. *Granular Matter*, 14(5), pp.621-638.
- Munjiza A., John N.W.M, Bangash T., 2004. The combined finite–discrete element method for structural failure and collapse. *Engineering Fracture Mechanics*, 71(4–6), pp.469-483.
- Nagai K., Sato Y., Ueda T., 2005. Mesoscopic Simulation of Failure of Mortar and Concrete by 3D RBSM. *Journal of Advanced Concrete Technology*, 3(3), pp.385-402.
- Nishiura D., Sakaguchi H., 2011. Parallel-vector algorithms for particle simulations on shared-memory multiprocessors. *Journal of Computational Physics*, 230, pp.1923-1938.
- Polojärvi A., Tuhkuri J., 2013. On modeling cohesive ridge keel punch through tests with a combined finite-discrete element method. *Cold Regions Science & Technology*, 85, pp.191-205.
- Potyondy D.O., Cundall P.A., 2004. A bonded-particle model for rock. *International Journal of Rock Mechanics & Mining Sciences*, 41(8), pp.1329-1364.
- Torquato S., Jiao Y., 2010. Dense packings of the Platonic and Archimedean solids, *Nature* 463, pp.876-879.
- Zhang J.H., He J.D, Fan J.W., 2001. Static and dynamic stability assessment of slopes or dam foundations using a rigid body–spring element method. *International Journal of Rock Mechanics & Mining Sciences*, 38(8), pp.1081-1090.
- Zhang X., 1999. Slope stability analysis based on the rigid finite element method. *Géotechnique*, 49(5), pp.585-593.
- Yue Q., Qu Y., Bi X., Karna T., 2005. Ice force spectrum on narrow conical structures. *Cold*

Regions Science & Technology, 49(2), pp.161-169.

Qu Y., Yue Q., Bi X., Karna T., 2006. A random ice force model for narrow conical structures.
Cold Regions Science & Technology, 45(3), pp.148-157.